

Dynamical properties of feedback signalling in B lymphopoiesis: A mathematical modelling approach

Salvador Chulián^{☆a,b}, Álvaro Martínez-Rubio^{☆a,b}, Anna Marciniak-Czochra^c,
 Thomas Stiehl^c, Cristina Blázquez Goñi^d, Juan Francisco Rodríguez
 Gutiérrez^d, Manuel Ramirez Orellana^e, Ana Castillo Robleda^e, Víctor M.
 Pérez-García^{f,g,h}, María Rosa^{a,b}

^a*Department of Mathematics, Universidad de Cádiz, Puerto Real, Cádiz, Spain*

^b*Biomedical Research and Innovation Institute of Cádiz (INiBICA), Hospital Universitario Puerta del Mar, Cádiz, Spain*

^c*Institute of Applied Mathematics, BioQuant and Interdisciplinary Center of Scientific Computing (IWR), Heidelberg University, Heidelberg, Germany*

^d*Department of Paediatric Haematology and Oncology, Hospital de Jerez Cádiz, Spain*

^e*Department of Paediatric Haematology and Oncology, Hospital Infantil Universitario Niño Jesús, Universidad Autónoma de Madrid, Madrid, Spain*

^f*Department of Mathematics, Mathematical Oncology Laboratory (MOLAB), Universidad de Castilla-La Mancha, Ciudad Real, Spain*

^g*Instituto de Matemática Aplicada a la Ciencia y la Ingeniería (IMACI), Universidad de Castilla-La Mancha, Ciudad Real, Spain*

^h*ETSI Industriales, Universidad de Castilla-La Mancha, Ciudad Real, Spain*

Abstract

Haematopoiesis is the process of generation of blood cells. Lymphopoiesis generates lymphocytes, the cells in charge of the adaptive immune response. Disruptions of this process are associated with diseases like leukaemia, which is especially incident in children. The characteristics of self-regulation of this process make them suitable for a mathematical study.

In this paper we develop mathematical models of lymphopoiesis using currently available data. We do this by drawing inspiration from existing structured models of cell lineage development and integrating them with paediatric bone marrow data, with special focus on regulatory mechanisms. A formal analysis of the models is carried out, giving steady states and their stability conditions. We use this analysis to obtain biologically relevant regions of the parameter space and to understand the dynamical behaviour of B-cell renovation. Finally, we

[☆]These authors contributed equally to this work.

use numerical simulations to obtain further insight into the influence of proliferation and maturation rates on the reconstitution of the cells in the B line. We conclude that a model including feedback regulation of cell proliferation represents a biologically plausible depiction for B-cell reconstitution in bone marrow. Research into haematological disorders could benefit from a precise dynamical description of B lymphopoiesis.

Keywords: Mathematical medicine, Haematopoiesis, Mathematical modelling, Lymphopoiesis

2010 MSC: 92B05, 92C15

1. Introduction

Blood is a tissue under continuous regeneration, and its renovation is one of the most studied developmental processes in biology [1]. It is initiated by haematopoietic stem cells and develops through a multi-step differentiation cascade [2], resulting in the generation of red blood cells, platelets and cells of the immune system. Figure 1(a) shows the standard representation of haematopoiesis as a tree. At the top, stem cells with the potential for self-renewal give rise to respective lineage progenitors. These cells become progressively more specialised as they move towards the bottom of the tree. There are two major cell lineages: the myeloid line and the lymphoid line. The latter generates lymphocytes, involved in adaptive immune response, which is responsible for ‘targeted’ reactions to infections.

In this work, we will focus on the description of B lymphopoiesis, i.e. the development and maturation of B cells. These cells have a range of roles, being mainly associated with the secretion of antibodies, the elements in charge of the neutralisation of foreign invaders [3]. Figure 1(b) shows a schematic representation of the route from common lymphoid progenitor to immature B cells, which eventually exit the bone marrow to complete maturation elsewhere. Alterations in the generation of B cells are related to diseases like autoimmune reactions, immunodeficiencies or lymphoproliferative disorders like lymphomas

or leukaemias [4]. The latter have especial incidence in children and constitute around one third of all childhood cancer cases [5].

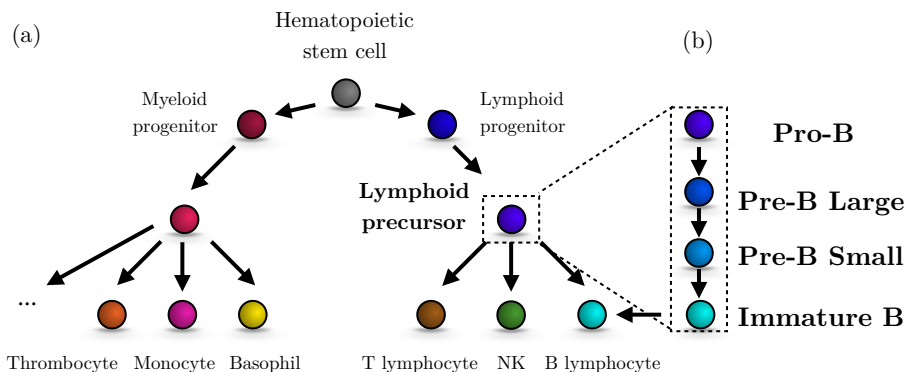


Figure 1: (a) Schematic representation of haematopoiesis. (b) B-cell lineage starts from a common lymphoid progenitor and then progresses towards immature B cells, which eventually leave the bone marrow. Hallmarks of this process are the acquisition of the immunophenotypic cell surface markers CD19 for the whole B line and CD10 for immature B cells.

Haematopoiesis is a perfect example of self-renewal and stemness in tissues [6]. Mathematical descriptions have been performed using multi-compartmental, continuously structured models [7, 8, 9]. In those models, each cell type in Figure 1(a) can be thought of as a cell compartment that receives input from the upper elements and sends its output to the lower compartments [10, 11, 12, 13, 14, 15, 39]. Some models have focused explicitly on the B-cell line [17, 18]. Unlike full haematopoiesis, this process is sequential, simplifying its mathematical conceptualisation. The compartmental models described above become nonlinear when the interactions between the different cell stages are included. Indeed, this process requires some kind of negative regulatory feedback in order to ensure steady production [19, 20]. This feature is common in the modelling of biological systems since they normally consist of a considerable number of interacting components [21].

In the case of B cells, their development depends on the joint action of a number of factors that support or inhibit B-cell growth and differentiation [22]. A clear description of the participants at each stage of development is lacking

[4], which is in part due to the difficulties in recreating *in-vivo* conditions in
40 experimental designs [23]. Mathematical models can help in elucidating which
processes are more influenced by a given type of signal, as has been done for a
number of lineages and scenarios [24, 25, 26, 27, 28], and a better comprehension
of these interactions can be useful in understanding progression to malignancies
[29].

45 In this context, a complete picture of B lymphopoiesis would be a useful
complement to those modelling scenarios that consider an input of B cells or that
represent B-cell-related phenomena [18, 30, 31, 32, 33]. Precise knowledge of the
dynamical behaviour of each stage of differentiation stage can also be of help
in clinical situations where disorders are especially linked to the characteristics
50 of the cell of origin. In leukaemias, for instance, the phenotype of the tumour
cells is an important diagnostic criterion [34]. Our aim in this paper is thus to
develop a model of B lymphopoiesis in the bone marrow. We will construct and
investigate the properties and dynamical behaviour of a series of models. This
will be complemented with data from the literature, which mainly comes from
55 *in-vitro* assays and immune reconstitution studies, and with clinical data from
haematological patients.

This paper is structured as follows: In Sec. 2 we explain basic haematological
models, going from a general model to a reduced family of models more suitable
for lymphopoiesis. In Sec. 3 we perform a mathematical analysis of these
60 models, including positivity, boundedness and stability. In Sec. 4 we carry out
numerical simulations, taking into account clinical data and information from
the literature. In Sec. 5 we discuss these results and examine the potential
of these models to describe the process, concluding with the kind of research
opportunities that this analysis paves the way for.

65 **2. Mathematical models and methods**

Our aim here is to describe B-cell development taking into account what the
data can tell us about the structure of the population of this haematopoietic

line. An illustration of the representation of cell development can be found in [35, 36], where the authors proposed n maturation stages for a cell population $u_n = u_n(t)$, with $t \in \mathbb{R}$ representing time. In this case, u_1 would represent stem cell population, u_n a mature specialised cell and u_i ($i = 2, \dots, n - 1$) intermediate stages.

The model was studied in terms of proliferation rates $p_i = p_i(t)$ and the so-called self renewal fraction $a_i = a_i(t)$, for each maturation stage $i = 1, \dots, n$. The latter is considered to be the probability of a cell remaining in the same cell compartment after mitosis. The authors assumed that cells at stage i enter mitosis with a rate p_i , resulting in a total number of $2p_i u_i$ after mitosis. Then, with probability a_i , they remain in the same compartment, whereas with probability $1 - a_i$ they go on to the next maturation stage. Therefore, each cell compartment has an output of $p_i u_i$ and an input $2p_i a_i u_i$ from their own compartment. Consequently, the previous compartment (except at the first stage) provides the input corresponding to the number of cells that go on to the next maturation stage after mitosis: $2p_{i-1}(1 - a_{i-1})u_{i-1}$. Lastly, mature cells die at a rate d , and they are not considered to enter mitosis. If we consider $n = 3$ stages for stem cells (u_1), intermediate cells (u_2) and specialised cells (u_3), the result is the following system of equations:

$$\frac{du_1}{dt} = p_1(2a_1 - 1)u_1, \quad (1a)$$

$$\frac{du_2}{dt} = p_2(2a_2 - 1)u_2 + 2p_1(1 - a_1)u_1, \quad (1b)$$

$$\frac{du_3}{dt} = 2p_2(1 - a_2)u_2 - du_3. \quad (1c)$$

B cells are far from the haematopoietic stem cells since they are already committed to the B line, thus losing part of their potential for self-renewal. We then choose to specify cell behaviour in each compartment in terms of proliferation and maturation, i.e. progression to the next stage, and to restrict the system to three different cell compartments, considering the most common immunophenotypical characterisation used in clinical practice [37]. The first compartment would also receive input from previous lymphoid progenitors. However, this

80 early compartment is smaller and thus a constant source term contribution would be less significant [38]. Furthermore, this input is also regulated, which would require adding an equation from the previous compartment, and similarly for even earlier compartments. Our aim was to restrict the analysis to the CD19⁺ fraction of the B-cell line, as suggested by the data (see Appendix A).

Thus we will consider three compartments accounting for the different maturation stages: early B cells ($C_1 = C_1(t)$), intermediate B cells ($C_2 = C_2(t)$), and finally late B cells ($C_3 = C_3(t)$), where $t \in \mathbb{R}$ represents time. A compartmental model can then be written as

$$\frac{dC_1}{dt} = \rho_1 C_1 - \alpha_1 C_1, \quad (2a)$$

$$\frac{dC_2}{dt} = \rho_2 C_2 + \alpha_1 C_1 - \alpha_2 C_2, \quad (2b)$$

$$\frac{dC_3}{dt} = \alpha_2 C_2 - \alpha_3 C_3. \quad (2c)$$

85 Note that this formulation is equivalent to the model from Eq. (1) with $u_i = C_i$ for $i = 1, 2, 3$ and parameters $\rho_i = p_i$, $\alpha_i = 2p_i(1 - a_i)$ for $i = 1, 2$, and $\alpha_3 = d$.

Early B cells, described here by Eq. (2a), have a proliferation rate ρ_1 and a transition rate into intermediate B cells of α_1 . Analogously, the proliferation 90 rate for intermediate B cells and transition rate into the late compartment are ρ_2 and α_2 , as described in Eq. (2b). In this equation, a fraction of $\alpha_1 C_1$ cells comes from the early B compartment. This also happens with the $\alpha_2 C_2$ cells that change their phenotypes from the intermediate B-cell into the late B-cell compartment. Late B cells in Eq. (2c) are not considered to enter mitosis and 95 they go into the blood flow with a blood transition rate α_3 .

This compartmental model needs to be complemented with a regulatory system involving cell feedback signalling $s(t)$. Different types of signalling and the importance of the regulation of self-renewal in homeostatic (steady) state have been previously studied in the literature [14, 19, 20, 24, 25, 26, 27]. In our case, there are different ways of specifying which cells participate in signalling 100 and through which processes. In this paper we consider two different hypotheses.

The first is that signals are produced either by late cells (model 1) or by all cells (model 2). The second is that signals can alternatively affect either the proliferation rate (model A) or the transition rate of the model (model B).
 105 Therefore, we will consider four possibilities regarding feedback signalling. This is summarized in Figure 2.

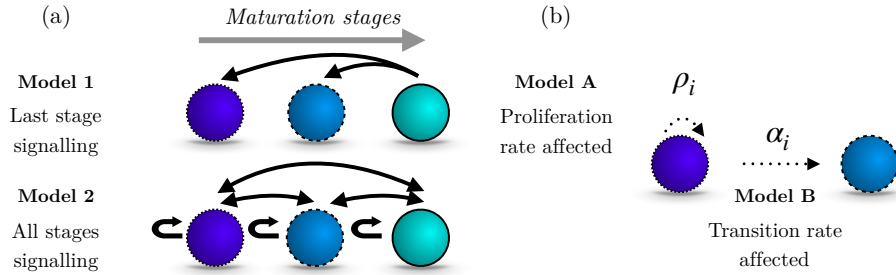


Figure 2: Representation of the different feedback signalling possibilities. (a) The signal may be produced by the most mature cells and then affect the previous compartments (model 1); or it may be produced by all cells, influencing the whole population (model 2). (b) Signalling can alternatively affect either the proliferation rate (model A) or the transition rate (model B).

As stated in the introduction, the precise number and role of interacting elements is unclear. The basic immune system chemical messengers are the cytokines, proteins that control cell production. They can be generated by
 110 microenvironmental elements but also from cells themselves [40]. For B cells, a number of cytokines have been shown to be relevant: IL-7 for proliferation, differentiation (transition) and survival [41], and SCF and FLT3LG [42] for proliferation of early stages [43]. Evidence in this regard comes mainly from *in-vitro* and murine models and differences with humans can be significant [23]. Due to
 115 this uncertainty and complexity we decided to follow an implicit formulation for the signalling as in [18], where instead of including each contributor explicitly we consider the systemic action of each, and gather them together in a single function $s(t)$.

With respect to the form of this signalling function $s(t)$, we follow the development set out in [35]. First, let us consider a maximal signal ρ_S , which is

self-limited with rate α_S . Consider then a number of cells $N = N(t)$ that regulates the production of this signal in such a way that it decreases when there is a large number. Thus, a general signalling $S = S(t)$ can be modelled as

$$\frac{dS}{dt} = \rho_S - \alpha_S S - \beta SN, \quad (3)$$

where β is the inhibitory influence of cells N . By making a change of variables $s(t) = \alpha_S/\rho_S \cdot S(t)$ and $k = \beta/\alpha_S$, we obtain a differential equation whose quasi-steady state is $s(t) = 1/(1 + kN(t))$. A rigorous analysis of this quasi-steady state approximation can be found in [44]. Signal concentration depends on the number of cells of type N . Following the explanation in Figure 2 we will consider the case when only the late cells participate in signalling, i.e.

$$s_1(t) = \frac{1}{1 + kC_3}, \quad (4)$$

or the case where all cells participate

$$s_2(t) = \frac{1}{1 + k \sum_{i=1}^3 C_i}. \quad (5)$$

Note that $s(t)$ is a decreasing function of the cell numbers C_i so it has an inhibitory role. The parameter k measures the strength of the inhibitory feedback.

To sum up, we will consider the models:

$$\frac{dC_1}{dt} = s_\rho \rho_1 C_1 - s_\alpha \alpha_1 C_1, \quad (6a)$$

$$\frac{dC_2}{dt} = s_\rho \rho_2 C_2 + s_\alpha \alpha_1 C_1 - s_\alpha \alpha_2 C_2, \quad (6b)$$

$$\frac{dC_3}{dt} = s_\alpha \alpha_2 C_2 - s_\alpha \alpha_3 C_3. \quad (6c)$$

Feedback signalling affects either proliferation (signal $s_\rho = s_\rho(t)$) or transition rates (signal $s_\alpha = s_\alpha(t)$). The form of the signals s_ρ, s_α depends on the signalling source, either $s_1(t)$ or $s_2(t)$. This yields four possible models, summarised in Table 1.

Signalling	1. Late cells	2. All Cells
A. Affecting proliferation	Model A1 ($s_\rho = s_1, s_\alpha = 1$)	Model A2 ($s_\rho = s_2, s_\alpha = 1$)
B. Affecting transition	Model B1 ($s_\rho = 1, s_\alpha = s_1$)	Model B2 ($s_\rho = 1, s_\alpha = s_2$)

Table 1: Mathematical models considered depending on signalling.

125 3. Theoretical results

3.1. Existence, boundedness and positivity of solutions

Models A can be written as

$$\frac{dC_1}{dt} = \frac{\rho_1 C_1}{1 + kN} - \alpha_1 C_1, \quad (7a)$$

$$\frac{dC_2}{dt} = \frac{\rho_2 C_2}{1 + kN} + \alpha_1 C_1 - \alpha_2 C_2, \quad (7b)$$

$$\frac{dC_3}{dt} = \alpha_2 C_2 - \alpha_3 C_3, \quad (7c)$$

and models B have the form

$$\frac{dC_1}{dt} = \rho_1 C_1 - \frac{\alpha_1 C_1}{1 + kN}, \quad (8a)$$

$$\frac{dC_2}{dt} = \rho_2 C_2 + \frac{\alpha_1 C_1}{1 + kN} - \frac{\alpha_2 C_2}{1 + kN}, \quad (8b)$$

$$\frac{dC_3}{dt} = \frac{\alpha_2 C_2}{1 + kN} - \frac{\alpha_3 C_3}{1 + kN}. \quad (8c)$$

Feedback signalling can depend on cells from the late stage with $N = C_3$ (models A1 and B1 with signal $s_1(t)$ as in Eq. (4)) or on all cells with $N = \sum_{i=1}^3 C_i$ (models A2 and B2 with signal $s_2(t)$ as in Eq. (5)).

Theorem 1. *Let us consider the following set*

$$Q = \{(C_1, C_2, C_3) \in \mathbb{R}^3 : C_1, C_2, C_3 > 0\}, \quad (9)$$

and the initial values in Q

$$C_1(t_0) = C_1^0, \quad C_2(t_0) = C_2^0, \quad C_3(t_0) = C_3^0, \quad (10)$$

130 Then, the initial value problem for either Eqs. (7) or Eqs. (8) has a unique local-in-time solution for each $t \in [t_0 - \epsilon, t_0 + \epsilon]$, for some value $\epsilon > 0$.

PROOF. The existence of a solution for systems from Eq. (7) and Eq. (8) is guaranteed for each $(C_1, C_2, C_3) \in Q$ by continuity of the functions

$$f_1^p = f_1^p(C_1, C_2, C_3) = \frac{\rho_1 C_1}{1 + kN} - \alpha_1 C_1, \quad (11a)$$

$$f_2^p = f_2^p(C_1, C_2, C_3) = \frac{\rho_2 C_2}{1 + kN} + \alpha_1 C_1 - \alpha_2 C_2, \quad (11b)$$

$$f_3^p = f_3^p(C_1, C_2, C_3) = \alpha_2 C_2 - \alpha_3 C_3, \quad (11c)$$

and

$$f_1^\alpha = f_1^\alpha(C_1, C_2, C_3) = \rho_1 C_1 - \frac{\alpha_1 C_1}{1 + kN}, \quad (12a)$$

$$f_2^\alpha = f_2^\alpha(C_1, C_2, C_3) = \rho_2 C_2 + \frac{\alpha_1 C_1}{1 + kN} - \frac{\alpha_2 C_2}{1 + kN}, \quad (12b)$$

$$f_3^\alpha = f_3^\alpha(C_1, C_2, C_3) = \frac{\alpha_2 C_2}{1 + kN} - \frac{\alpha_3 C_3}{1 + kN}, \quad (12c)$$

where again $N = C_3$ or $N = \sum_{i=1}^3 C_i$. Boundedness of the respective partial derivatives of f_i^α and f_i^p for $i = 1, 2, 3$ proves that they satisfy the Lipschitz conditions, and therefore the solutions of systems from Eq. (7) and Eq. (8)

135 with initial values as in Eq. (10) are unique by the Picard-Lindelöf theorem.

Henceforth we will consider that all parameters ρ_i, α_i and initial conditions C_i^0 are positive for $i = 1, 2, 3$.

Theorem 2. *The solutions of Eqs. (7) and Eqs. (8) with $(C_1^0, C_2^0, C_3^0) \in Q$ are positive.*

PROOF. Let us consider the functions f_i^p, f_i^α with $i = 1, 2, 3$ from Eqs. (11) and Eqs. (12), respectively. As $f_i^p, f_i^\alpha > -\alpha_i C_i$, we know that

$$\frac{dC_i}{dt} > -\alpha_i C_i. \quad (13)$$

By integrating both sides of the equation from t_0 to t we obtain

$$C_i(t) > C_i^0 \exp(-\alpha_i t) > 0. \quad (14)$$

140 And therefore all solutions $C_i(t)$, $i = 1, 2, 3$ are positive over their domain of definition.

Theorem 3. *The solutions $C_1(t), C_2(t), C_3(t)$ of Eqs. (7) with $(C_1^0, C_2^0, C_3^0) \in Q$ are bounded.*

PROOF. In model from Eq. (7) if we consider C_1 to be unbounded, then

$$\lim_{C_1 \rightarrow \infty} \frac{dC_2}{dt} = \infty, \quad (15)$$

which would imply that C_2 would also be unbounded, and analogously for the case of C_3 . We could then write

$$\lim_{C_i \rightarrow \infty} \frac{C_i}{1 + kC_3} = \lim_{C_i \rightarrow \infty} \frac{C_i}{1 + k \sum_{j=1}^3 C_j} = \frac{1}{k} \quad \text{for } i = 1, 2, 3. \quad (16)$$

Let us now consider the functions f_i^ρ from Eq. (11). From Eq. (16) we get

$$f_1^\rho < \frac{\rho_1}{k} - \alpha_1 C_1, \quad (17)$$

and then for all t

$$C_1 < Ae^{-\alpha_1 t} + \frac{\rho_1}{k\alpha_1}, \quad A \in \mathbb{R}, \quad (18)$$

which yields that $C_1(t)$ is bounded. Considering $C_1(t) < M_1 \in \mathbb{R}$, for all t , then

$$f_2^\rho < \frac{\rho_2}{k} + \alpha_1 M_1 - \alpha_2 C_2, \quad (19)$$

and integrating as above implies C_2 is bounded. Considering $C_2 < M_2 \in \mathbb{R}$,

$$f_3^\rho < \alpha_2 M_2 - \alpha_3 C_3, \quad (20)$$

and thus C_3 is also bounded.

For the models B, ruled by Eqs. (8), we can sum the three equations to obtain

$$\frac{dC_T}{dt} = \rho_1 C_1 + \rho_2 C_2 - \frac{\alpha_3 C_3}{1 + kN}, \quad (21)$$

145 where $C_T = C_1 + C_2 + C_3$. It is clear that for C_1 and C_2 sufficiently large the negative term makes only a small contribution and thus solutions are not bounded. This implies that models in which signalling affects only transition rates are not appropriate for representing biological processes of this kind.

3.2. Steady States and stability conditions

150 Biological processes in homeostasis are stable and robust. In addition to being mathematically well posed, we need to ensure that the models have a positive stable equilibrium in which the three populations coexist. In this section we study the existence of such states and their local stability. We focus on models A (Eq. (7)), since models B (Eq. (8)) do not lead to biologically 155 relevant dynamics. An expanded analysis of the stability conditions for certain steady states of models A can be found in Appendix B. Further analysis of models B, showing that they have only unstable non-trivial positive equilibria, is presented in Appendix C.

3.2.1. Model A1

Let us consider last stage signalling $s_\rho = s_1(t)$ as in Eq. (4) affecting the proliferation term, i.e. we study Eq. (7) with $N = C_3$. The three steady states for this model are

$$P_1^{A1} = (0, 0, 0), \quad (22a)$$

$$P_2^{A1} = \left(0, \frac{\alpha_3(\rho_2 - \alpha_2)}{k\alpha_2^2}, \frac{\rho_2 - \alpha_2}{k\alpha_2} \right), \quad (22b)$$

$$P_3^{A1} = \left(\frac{\alpha_3(\rho_1 - \alpha_1)(\alpha_2\rho_1 - \alpha_1\rho_2)}{k\alpha_1^2\alpha_2\rho_1}, \frac{\alpha_3(\rho_1 - \alpha_1)}{k\alpha_1\alpha_2}, \frac{\rho_1 - \alpha_1}{k\alpha_1} \right). \quad (22c)$$

The Jacobian matrix of the system at any point (C_1, C_2, C_3) is

$$J_{A1}(C_1, C_2, C_3) = \begin{pmatrix} \frac{\rho_1}{C_3k+1} - \alpha_1 & 0 & -\frac{C_1k\rho_1}{(C_3k+1)^2} \\ \alpha_1 & \frac{\rho_2}{C_3k+1} - \alpha_2 & -\frac{C_2k\rho_2}{(C_3k+1)^2} \\ 0 & \alpha_2 & -\alpha_3 \end{pmatrix}. \quad (23)$$

Substituting $P_1^{A1} = (0, 0, 0)$ in Eq. (23) we get the eigenvalues

$$\lambda_{1,1}^{A1} = -\alpha_3, \quad (24a)$$

$$\lambda_{1,2}^{A1} = \rho_1 - \alpha_1, \quad (24b)$$

$$\lambda_{1,3}^{A1} = \rho_2 - \alpha_2. \quad (24c)$$

This is the trivial equilibrium that would be unstable in normal homeostatic processes. Instability conditions are

$$\rho_1 > \alpha_1, \text{ or } \rho_2 > \alpha_2. \quad (25)$$

160 As we consider $P_2^{A1} > 0$, it must be $\rho_2 > \alpha_2$, and therefore P_1^{A1} is unstable.

For P_2^{A1} , we obtain

$$\lambda_{2,1}^{A1} = \frac{\alpha_2 \rho_1}{\rho_2} - \alpha_1, \quad (26a)$$

$$\lambda_{2,2}^{A1} = -\frac{\alpha_3}{2} - \frac{\sqrt{\alpha_3(4\alpha_2^2 - 4\alpha_2\rho_2 + \alpha_3\rho_2)}}{2\sqrt{\rho_2}}, \quad (26b)$$

$$\lambda_{2,3}^{A1} = -\frac{\alpha_3}{2} + \frac{\sqrt{\alpha_3(4\alpha_2^2 - 4\alpha_2\rho_2 + \alpha_3\rho_2)}}{2\sqrt{\rho_2}}. \quad (26c)$$

This equilibrium point corresponds to a situation where the less differentiated compartment disappears and the system is maintained only by the proliferation of the second, leading to mature cells. As before, this is not a biologically feasible situation, thus this equilibrium must be unstable. Since $\mathcal{R}(\lambda_{2,2}) < 0$ and $\mathcal{R}(\lambda_{2,3}) < 0$, then $\frac{\alpha_2 \rho_1}{\rho_2} - \alpha_1 > 0$, which means that for P_2^{A1} to be unstable we must have

$$\alpha_2 \rho_1 - \alpha_1 \rho_2 > 0. \quad (27)$$

From the positivity of the non-trivial equilibrium point P_3^{A1} we require

$$\rho_1 > \alpha_1, \quad (28a)$$

$$\frac{\rho_1}{\rho_2} > \frac{\alpha_1}{\alpha_2}. \quad (28b)$$

Conditions (28b) and (27) are identical which means that the existence of this positive equilibrium implies the instability of P_2^{A1} . Stability conditions for P_3^{A1} are lengthy and can be found in Appendix B.

3.2.2. Model A2

Model A2 is given by Eqs. (7) with $N = \sum_{i=1}^3 C_i$. The equilibria are

$$P_1^{A2} = (0, 0, 0), \quad (29a)$$

$$P_2^{A2} = \left(0, \frac{\alpha_3(\rho_2 - \alpha_2)}{k\alpha_2(\alpha_2 + \alpha_3)}, \frac{\rho_2 - \alpha_2}{k(\alpha_2 + \alpha_3)} \right), \quad (29b)$$

$$P_3^{A2} = \left(\frac{\alpha_3(\rho_1 - \alpha_1)(\alpha_2\rho_1 - \alpha_1\rho_2)}{\alpha_1k\beta}, \frac{\alpha_3\rho_1(\rho_1 - \alpha_1)}{k\beta}, \frac{\alpha_2\rho_1(\rho_1 - \alpha_1)}{k\beta} \right), \quad (29c)$$

where

$$\beta = (\alpha_2\alpha_3\rho_1 + \alpha_1(\alpha_2\rho_1 + \alpha_3(\rho_1 - \rho_2))). \quad (30)$$

The Jacobian matrix is

$$J_{A2} = \begin{pmatrix} -\alpha_1 + (s^{-1} - kC_1)s^2\rho_1 & -C_1ks^2\rho_1 & -C_1ks^2\rho_1 \\ \alpha_1 - C_2ks^2\rho_2 & -\alpha_2 + (s^{-1} - kC_2)s^2\rho_2 & -C_2ks^2\rho_2 \\ 0 & \alpha_2 & -\alpha_3 \end{pmatrix}. \quad (31)$$

Substituting P_1^{A2} in Eq. (31) we obtain

$$\lambda_{1,1}^{A2} = -\alpha_3, \quad (32a)$$

$$\lambda_{1,2}^{A2} = \rho_1 - \alpha_1, \quad (32b)$$

$$\lambda_{1,3}^{A2} = \rho_2 - \alpha_2. \quad (32c)$$

165 As before, for this equilibrium to be unstable we should have either $\rho_1 > \alpha_1$ or/and $\rho_2 > \alpha_2$. From the positivity of P_2^{A2} , it must be the case that $\rho_2 > \alpha_2$.

For P_2^{A2} , we obtain the eigenvalues

$$\lambda_{2,1}^{A2} = \frac{\alpha_2\rho_1}{\rho_2} - \alpha_1, \quad (33a)$$

$$\lambda_{2,2}^{A2} = \frac{\alpha_2^2\alpha_3 - 2\alpha_2\alpha_3\rho_2 - \alpha_3^2\rho_2 + h(\alpha_2, \alpha_3, \rho_2)}{2\rho_2(\alpha_2 + \alpha_3)}, \quad (33b)$$

$$\lambda_{2,3}^{A2} = \frac{\alpha_2^2\alpha_3 - 2\alpha_2\alpha_3\rho_2 - \alpha_3^2\rho_2 - h(\alpha_2, \alpha_3, \rho_2)}{2\rho_2(\alpha_2 + \alpha_3)}. \quad (33c)$$

where $h = h(\alpha_2, \alpha_3, \rho_2)$ such that

$$h = \sqrt{\alpha_3} \sqrt{2\alpha_2^2\alpha_3(\alpha_3 - 2\rho_2)\rho_2 + 4\alpha_2^3(\alpha_3 - \rho_2)\rho_2 + \alpha_3^3\rho_2^2 + \alpha_2^4(\alpha_3 + 4\rho_2)}. \quad (34)$$

As in the previous model, the existence of P_3^{A2} as a positive equilibrium influences the stability of P_2^{A2} . For the positivity of P_3^{A2} we have a first set of conditions

$$\beta > 0, \tag{35a}$$

$$\rho_1 > \alpha_1, \tag{35b}$$

$$\alpha_2 \rho_1 > \alpha_1 \rho_2; \tag{35c}$$

or a second set of conditions

$$\beta < 0, \tag{36a}$$

$$\rho_1 < \alpha_1, \tag{36b}$$

$$\alpha_2 \rho_1 < \alpha_1 \rho_2. \tag{36c}$$

Let us first consider that Eq. (35) holds. Then, in Eq. (33), the eigenvalue $\lambda_{2,1}^{A2}$ is positive and P_2^{A2} would be unstable. On the other hand, if Eq. (36) holds, then in Eq. (33) the eigenvalue $\lambda_{2,1}^{A2} < 0$. Then P_2^{A2} would be stable whenever

$$|\mathcal{R}(h)| > \alpha_2^2 \alpha_3 - 2\alpha_2 \alpha_3 \rho_2 - \alpha_3^2 \rho_2 \tag{37}$$

for h as defined in Eq. (34).

In this case, for the stability of P_2^{A2} , the difference with model A1 is the existence of a denominator β (Eq. (30)). The stability conditions for P_3^{A2} are not shown here for reasons of space, but they are presented in Appendix B. Stability conditions related to model B, as well as a summary of all the stability conditions depending on both models, can be found in Appendix C and Appendix D, respectively.

4. Numerical results

4.1. Parameter estimation

In the models presented above there are two parameters related to proliferation ρ_i ($i = 1, 2$), three related to compartmental transitions α_i ($i = 1, 2, 3$), and another related to the strength of signalling, the inhibition constant k .

A direct measure of the proliferation rates for the specific subsets considered
 180 in this paper is lacking, but we can provide an estimation based on qualitative
 biological information. Normal B-cell development can be compared to data
 from autologous bone marrow transplantation. This type of transplantation is
 more likely to reproduce developmental ontogeny, especially if there is no prior
 or adjuvant anti-B-cell therapy [45]. In this case B-cell progenitors can be
 185 detected in bone marrow as early as 1 month after transplantation [46, 47], and
 in blood after some delay [48]. *In-vitro* studies with mice show that proliferation
 rates are of the order of magnitude of days [40, 49, 50]. Human lymphoid
 cultures suggest doubling times of 1 day [51]. With respect to the relative values,
 current schemes for B-cell maturation indicate that upon CD19 acquisition there
 190 is sustained proliferation that decreases as the cell matures [40, 52, 53]. Late
 B cells already express B-cell receptor and a negative selection process occurs
 prior to this [22, 54]. Based on this we can consider that the net production
 rate of intermediate cells is lower than early cells ($\rho_1 > \rho_2$).

In order to obtain values for transition rates we make use of steady state
 expressions given by (22c) or (29c). These values can be compared to the flow
 cytometry data of normal bone marrow (See Appendix A). However, in our
 simulations we are measuring absolute cell counts while flow cytometry is only
 able to measure relative cell proportions. The positive non-trivial equilibrium
 (C_1^*, C_2^*, C_3^*) given by (22c) or (29c) satisfies the relationships

$$\frac{C_2^*}{C_3^*} = \frac{\alpha_3}{\alpha_2}, \quad (38a)$$

$$\frac{C_1^*}{C_2^*} = \frac{\alpha_2 \rho_1 - \alpha_1 \rho_2}{\alpha_1 \rho_1}. \quad (38b)$$

These quantities can be obtained from the analysis of the relative abundance
 195 of the three different populations. Thus, for each blood transition rate α_3 we
 can obtain values of α_1, α_2 that agree with steady-state data and at the same
 time belong in the positive stability region of parameter space. An example
 of the correlation found between transition rates is shown in Figure 3. The
 order of magnitude of α_3 can be estimated as follows. The term $\alpha_3 C_3^*$ gives

200 the total number of B cells per hour sent to blood by the bone marrow in
homeostatic circumstances. In mice, bone marrow produces around 0.1% of
the steady state population per hour [55]. In humans, the total steady-state
B-lymphocyte population can be obtained from lymphocyte proportions and
bone-marrow volumes from the literature and we estimate it to be 10^{10} cells
205 [56, 57, 58, 59, 60]. This yields a B-cell production of 10^7 cells per hour, and
given that $C_3^* \sim 10^9$ we estimate α_3 to be of the order of magnitude of 10^{-2} h^{-1} .

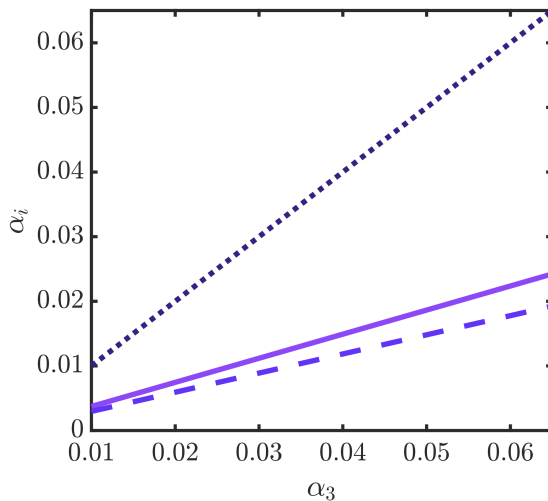


Figure 3: Dependence of the transition rates over the range of stability. Lines represent α_1 (light purple solid line), α_2 (purple dashed line), α_3 (dark purple dotted line). Across this range α_j satisfies the relationship $\alpha_3 > \alpha_1 > \alpha_2$. Values computed from Eq. (38) with $\rho_1 = 0.0289 \text{ h}^{-1}$, $\rho_2 = 0.0193 \text{ h}^{-1}$ and steady-state cell proportions $C_1^*/C_2^* = 0.0986$ and $C_2^*/C_3^* = 3.227$.

The last parameter to be determined is the inhibition constant k . Inspection of steady states shows that, given transition and proliferation rates of the order of magnitude of days, k is of the order of magnitude of the inverse of the total
210 steady-state population $k \propto (C_1^* + C_2^* + C_3^*)^{-1}$. The precise values for k and
 α_3 are selected so that we recover steady-state values and reconstitution times
compatible with the literature cited above. Ranges of parameters in agreement
with positivity, stability and steady-state conditions are shown in Table 2.

Param.	Meaning	Value	Units
ρ_1	Early B proliferation rate	$\ln(2)/24$	hours ⁻¹
ρ_2	Intermediate B proliferation rate	$\ln(2)/36$	hours ⁻¹
α_1	Transition rate: early to intermediate	(0.004, 0.025)	hours ⁻¹
α_2	Transition rate: intermediate to late	(0.003, 0.02)	hours ⁻¹
α_3	Transition rate: late to blood	(0.01, 0.065)	hours ⁻¹
k	Inhibition constant	(10^{-11} , 10^{-10})	cells ⁻¹

Table 2: Parameter values for Eqs. (7).

With respect to the initial state, the absolute number of mononucleated
215 transplanted cells (MNC) is in the range of 10^9 cells [48]. From these cells,
only a 1% are B early cells (10^7 cells) [38, 61]. These cells travel through blood
into the bone marrow but only 10% of cells eventually reach the bone marrow
[62]. Therefore, we will consider for the numerical simulations of autologous
transplantation an initial absolute number of cells of $C_1(0) = 10^6$, $C_2(0) = 0$,
220 $C_3(0) = 0$. The influence of this initial value on the dynamics of the system is
described in Sec. 4.3.

4.2. Global feedback signalling results in a smoother transition to steady states.

Typical results of simulations of models A1 and A2 (Eq. (7)) are shown in
Figure 4. Recall that in model A1 (Figure 4(a)) the signal depends only on cells
225 in the final compartment while in model A2 (Figure 4(b)) all cells are involved.
Both models exhibit qualitatively similar behaviour. Early cells appear first,
reaching a peak in population numbers slightly before day 30. Intermediate
cells follow, reaching the respective peak with days of delay and with larger
cell numbers. Late cells appear last and stabilize in between. The system
230 settles into the steady state from day 80 onwards. This behaviour agrees with
the conditions expressed above for the parameter values. In particular, the
proportion of population from each stage is coherent with clinical data (See
Appendix A) and experimental data [38]. For both models we have 8.99%
early cells, 70.21% intermediate cells and 20.80% late cells.

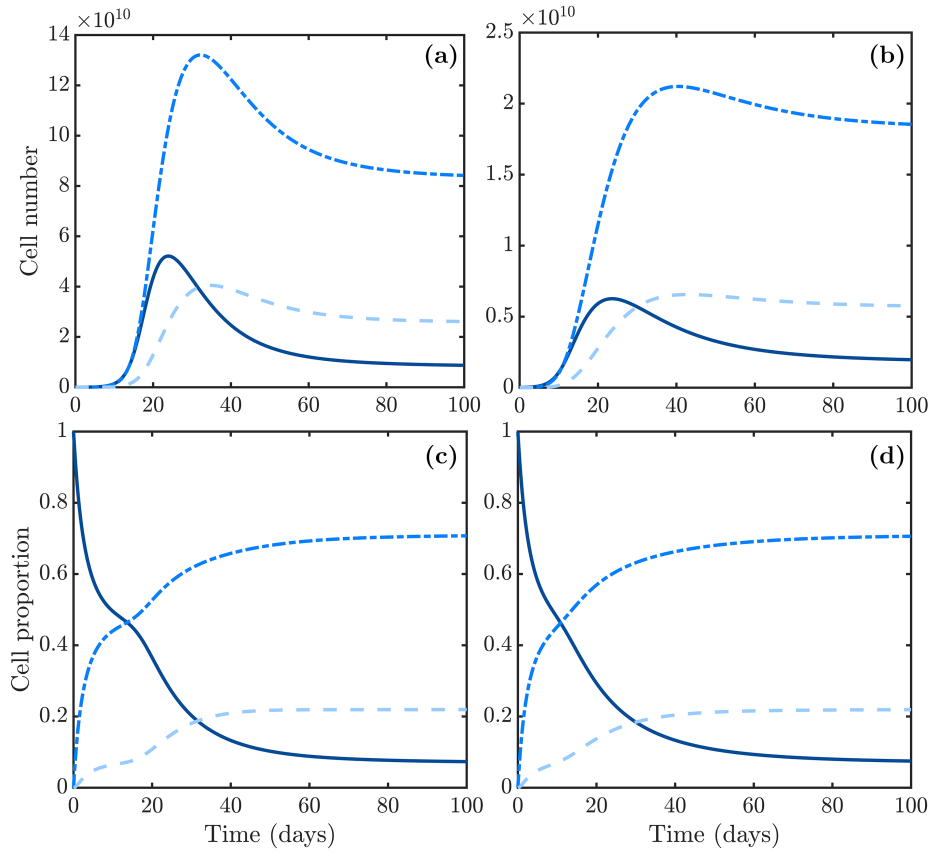


Figure 4: Comparison of numerical solutions of models A1 (a) and A2 (b) (Eq. (7)) and relative proportions (c) and (d), respectively, during the first 100 days. Curves represent early cells C_1 (dark blue solid line), intermediate cells C_2 (blue dashed-dotted line) and late cells C_3 (light blue dashed line). Both simulations have initial data $C_1(0) = 10^6$, $C_2(0) = 0$, $C_3(0) = 0$ cells and parameter values $\rho_1 = 0.0289 \text{ h}^{-1}$, $\rho_2 = 0.0193 \text{ h}^{-1}$, $\alpha_1 = 0.008 \text{ h}^{-1}$, $\alpha_2 = 0.006 \text{ h}^{-1}$, $\alpha_3 = 0.02 \text{ h}^{-1}$ and $k = 10^{-10}$.

235 There are two main differences between the two models. The first relates to
the magnitude of the steady state, which is larger when only late cells participate
in signalling (model A1, Figure 4(a)) for the same parameter values. This can
be observed in Figure 5(a), where total cell numbers for both models are shown.
Note that peak lymphocyte count, i.e. the largest cell number, occurs at day
240 30, when intermediate cells are maximal. The second difference relates to the

early behaviour of the reconstitution. In global signalling simulation (model A2, Figure 4(b)) there is a much less pronounced peak than when only late cells perform the signalling, presenting a smoother transition to the equilibrium state.

245 Figures 4(c) and (d) show the evolution of the percentage of each maturation stage. It is interesting to relate this to absolute counts since, as explained in Sec. 4.1, flow cytometry data only captures relative cell proportions. We observe very close behaviour between the models. The percentage of early cells quickly decreases as more mature stages appear and steady-state proportions
 250 are reached from day 80 onwards. Note that even though intermediate and mature cells have a peak in absolute cell count, this peak is not represented in terms of percentage. Also, this figure shows that a decrease in cell percentage does not necessarily means a decrease in absolute cell count, something to take into account when interpreting longitudinal flow cytometry data.

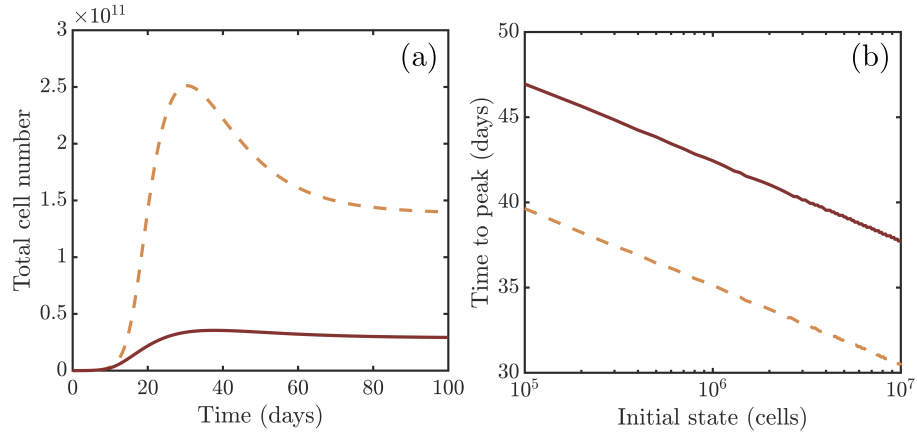


Figure 5: Comparison of numerical simulations of model A1 (orange solid line) and A2 (red dashed line) from Eq. (7) for: (a) total number of cells $C_1 + C_2 + C_3$, with initial cell numbers $C_1(0) = 10^6$, $C_2(0) = 0$, $C_3(0) = 0$; (b) time to peak lymphocyte count as a function of initial early B cell number. Both simulations have parameter values $\rho_1 = 0.0289 \text{ h}^{-1}$, $\rho_2 = 0.0193 \text{ h}^{-1}$, $\alpha_1 = 0.008 \text{ h}^{-1}$, $\alpha_2 = 0.006 \text{ h}^{-1}$, $\alpha_3 = 0.02 \text{ h}^{-1}$ and $k = 10^{-10}$.

255 *4.3. Time to peak decreases exponentially with initial value*

In Sec. 4.1 we described the rationale for the choice of the initial value of early cells. Despite this, we sought to determine how the scale of this data impacted reconstitution times. In Figure 5(b) we show the time to peak cell count for a range of initial values for early cells. There exists a decreasing exponential relationship between the two magnitudes, although the delay is not significant when considering that the literature on reconstitution after autologous transplantation describes reconstitution times in the range of 1-2 months [46]. Multiplying initial cell numbers by 10 results in a displacement in time of 5 days.

265 *4.4. Blood transition rate influences time to bone marrow reconstitution*

Clinical data suggests that homeostatic bone marrow displays relatively constant subset proportions (See Appendix A). This, together with the analysis of the expressions of the steady states allowed us to derive a connection between the three transition rates in the model (Eq. 38). For the ranges of parameters considered, we observed that $\alpha_3 > \alpha_1 > \alpha_2$ (see Figure 3), which suggests that the second compartment being more numerous could be due not to a higher proliferation rate but rather to a slower maturation time. This calls for the analysis of the influence of transition rates on the dynamics of the system.

In order to do this we focused on variations of α_3 , the rate at which late cells exit bone marrow and enter the blood flow. We select a range of variation that lies in the positive stability region and observe the qualitative differences in the immune reconstitution. Results are shown in Figure 6(a).

We observe that an increasing blood transition rate means that the system reaches a lower number of total cells. Indeed, Eq. (22) shows that population levels depend on transition rates. Note that the peak during reconstitution also decreases. In order to quantify this reduction, we show, in Figure 6(b), the proportion of the height of the peak with respect to the final steady state, for the same range of values for α_3 . For lower values of blood transition rate, the transitory population of lymphocytes can be 1.3 times the population in

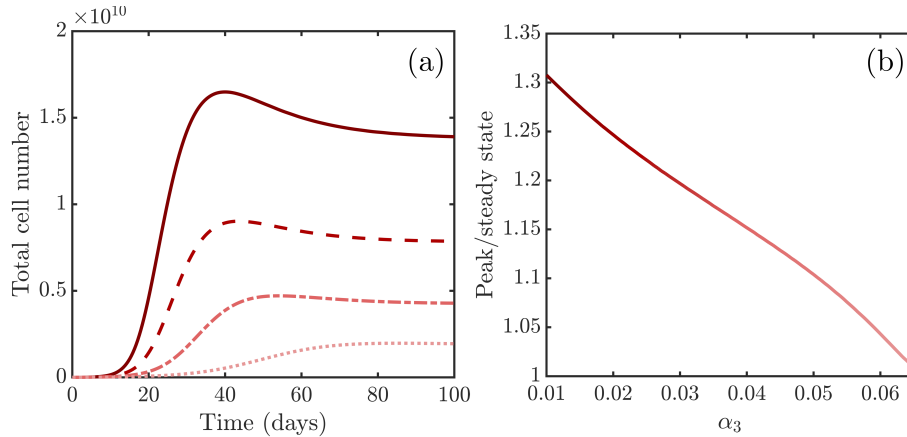


Figure 6: Numerical simulations for variable blood transition rate. (a) Total cell number $C_1 + C_2 + C_3$ for $t \in [0, 100]$ days. Blood transition rate values: $\alpha_3 = 0.03 \text{ h}^{-1}$ (solid line), $\alpha_3 = 0.04 \text{ h}^{-1}$ (dashed line), $\alpha_3 = 0.05 \text{ h}^{-1}$ (dashed-dotted line), $\alpha_3 = 0.06 \text{ h}^{-1}$ (dotted line). Line colour goes from dark red to pink as blood transition rate increases. (b) Peak to steady state value ratio for the same range of blood transition rates. Both simulations belong to model A2 (Eq. (7)) with initial state $C_1(0) = 10^6$, $C_2(0) = 0$, $C_3(0) = 0$ cells and parameter values $\rho_1 = 0.0289 \text{ h}^{-1}$, $\rho_2 = 0.0193 \text{ h}^{-1}$ and $k = 10^{-10}$. Parameters α_2 and α_1 vary with α_3 according to Eq. (38).

285 homeostatic conditions. This proportion decreases if cells increase the rate at which they join blood flow. Another consequence coming from these numerical simulations is that the lower the transition rates, the longer it takes for the system to stabilise.

4.5. Inhibition constant has no qualitative impact on the dynamical process

290 Eq. (22) shows that steady state values depend on transition rates (see also Figure 6) but also on the inhibition constant k . To quantify the impact of the parameter k on the dynamics of the system, we computed the total steady-state cell number as well as the proportion of peak height to steady state in a range of α_3 (and thus α_1 and α_2) and k values. The results are shown in Figure 7 for
 295 model A2. With respect to the absolute final cell count, only low levels of both k and α_3 result in a much higher number of cells. We highlighted an area for which the total cell amount C_T is in the range $(10^{10}, 10^{11})$, as estimated in Sec.

4.1 from reference values. For the proportion of peak height to steady state, there is little variation in the direction of k , so signalling intensity has little influence on the dynamics. As shown in Figure 6, high peak values belong in the low blood transition rate area. We conclude that transition rates primarily cause the overshoot during reconstitution, while k is mainly responsible for the existence of stability regimes and the size of the final states.

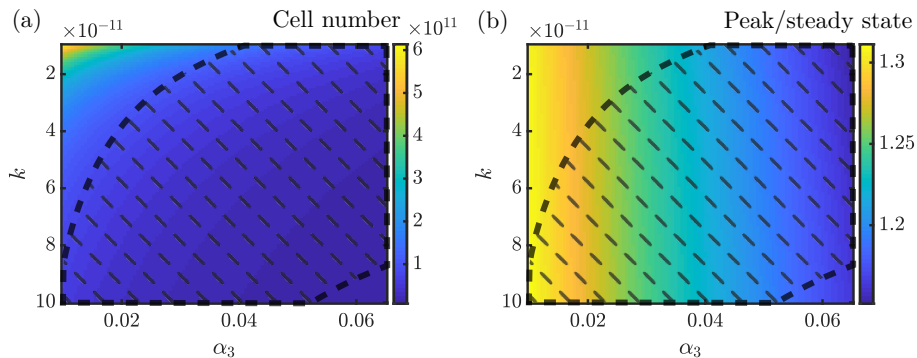


Figure 7: Influence of inhibition constant k and blood transition rate α_3 parameters in model A2 (Eq. (7) with all cell signalling) for (a) total steady state cell number, (b) peak vs steady states ratio. The dashed highlighted area represents the range in which total cell number $C_T \in (10^{10}, 10^{11})$. Each coordinate is the result of a numerical simulation of model A2 with initial state cell numbers $C_1(0) = 10^6$, $C_2(0) = 0$, $C_3(0) = 0$ and parameter values $\rho_1 = 0.0289 \text{ h}^{-1}$ and $\rho_2 = 0.0193 \text{ h}^{-1}$. Parameters α_1 and α_2 vary with $\alpha_3 \in (0.01 \text{ h}^{-1}, 0.03 \text{ h}^{-1})$ as explained in Eq. (38).

5. Discussion and conclusions

Haematopoiesis is one of the most widely studied biological developmental processes [1]. Interesting questions arise related to the processes of cell lineage specification [2, 63], the role of stem cells [6, 64] and the way cells communicate to regulate and ensure steady production [65, 66]. This is also true for B lymphopoiesis, the branch of haematopoiesis pertaining to B-cell formation. Specific unknowns in B-cell biology are the origins of some developmental stages, the role of senescence or the array of cytokines that regulates this process [67].

Studies of human B lymphopoiesis are encouraged, given that most of our knowledge about this line comes from mouse models [4]. Answering these questions and obtaining a precise description of the dynamics of B-cell maturation are
315 fundamental for research avenues. Some examples are the characterisation of haematological malignancies, the reconstitution after bone marrow transplant or chemotherapy or the generation of new lymphocytes from human embryonic stem cells [67].

Mathematical models have the potential to integrate biological hypotheses
320 and clinical data in order to provide an abstract representation of biological processes [11]. This representation can be useful not only for understanding the dynamical properties of the system, but also for testing and elucidating more inaccessible phenomena. Our goal in this paper was to establish a biologically sensible mathematical characterization of the B lymphopoiesis. Spurred
325 by previous models of haematopoietic processes [14, 35], we designed four models each with three differentiation stages. We added an implicit and systemic consideration of cell feedback signalling resulting in four nonlinear models. We first analysed these models from a theoretical perspective, addressing existence, positivity, boundedness and local stability. We collected data from the literature and clinical data from haematological patients and then used numerical
330 simulations in order to understand the role and influence of each parameter.

We learn from theoretical analysis that a stable, homeostatic situation cannot arise solely by regulating the transition rate, i.e. the process of differentiation or maturation to the next compartment. We have focused from there
335 onward on feedback regulation of cell proliferation. Inspection of the steady states allowed us to use flow cytometry data to establish a relationship between the three transition rates, analysing their influence by manipulating them one by one. The relationship suggests that, for the specific cell proportions in the B line, cells transition faster from early to intermediate than from intermediate
340 to late. Intermediate cells could then be more numerous not because they proliferate more, but because of their slower transition rates downstream towards more mature cell types. Also, numerical simulations show that cell proportion

is independent of which cells perform the signalling.

In this sense, we observed that signalling coming from all stages results in
345 a smoother reconstitution of the B cell line. Indeed, when all populations participate in signalling, their influence occurs earlier and proliferation decreases faster with time than when only late cells do. In this case we observed a peak that we understood as a consequence of the delay in the reaction of the system to overpopulation. The amplitude of this peak is also correlated with lower
350 transition rates, which implies lower steady states values. This is biologically understandable: the late compartment saturates due to excessive input from previous compartments, delaying access to stability and thus maintaining cell production in upstream compartments. It is important to remark here that subset percentage, a common metric in follow-up samples in a clinical context,
355 can be misleading when dynamics of expansion are at play. For example, the overshoot during early reconstitution is not observed in terms of relative proportions. Finally, we noted that the strength of the signalling has no impact on the dynamics. The feedback loop could then be understood as a mechanism for the existence of stable output, while dynamical characteristics (time to
360 reconstitution or early peak) are more dependent on intrinsic cellular processes.

The idea of this study was to determine which conditions are sufficient, from a mathematical perspective, to represent the kind of biological data that is currently available for B-line development. While we obtain a behaviour that fits with the time scales of the *in-vivo* process [45, 46, 47, 48, 51, 38], our study has a
365 series of limitations. Firstly, the choice of three compartments could be refined or expanded following a more detailed characterisation of the cells. Multidimensional flow cytometry data shows that surface markers, those that specify to which stage a given cell belongs, vary continuously. A mathematical model where these markers vary continuously might be able to capture this variation.
370 Secondly, we described signalling as a systemic phenomenon. While this was enough to recapitulate known B-cell behaviour, a more detailed description including two or more types of signalling is desirable. Lastly, the model would benefit from longitudinal data coming from immune reconstitution of the B-cell

line. In this regard, flow cytometry analyses of both peripheral blood and bone
375 marrow in routine follow-up would allow for a more precise parameterisation
and enable the hypotheses presented above to be contrasted.

To conclude, we have constructed and studied several non-linear compart-
mental models describing B cell lymphocyte reconstitution. These simple mod-
els describe the process of B-cell generation as portrayed by bone marrow data,
380 and we consider it a first step in a deeper exploration of the phenomena associ-
ated with B-cell development. We verified mathematical and biological consis-
tence, opening the door to interesting mathematical research like the existence
of bifurcations or the conditions for global stability, something that finds im-
mediate application in cases of immune reconstitution. Studies of this kind can
385 function as a source of hypothesis generation in biomedical research, for example
when contrasting mouse versus human dynamics. Ultimately, we aim to extend
the methodology to situations of stability disruption and abnormal growth like
B-cell disorders and other haematological diseases.

Acknowledgements

390 The support of the Junta de Andalucía group FQM-201 is gratefully ac-
knowledged. This work has been partially supported by the Fundación Española
para la Ciencia y la Tecnología (FECYT, project PR214 from the University of
Cádiz) and the Asociación Pablo Ugarte (APU). This work has been partially
supported by the Junta de Comunidades de Castilla-La Mancha (grant number
395 SBPLY/17/180501/000154).

Appendix A. Data

Appendix A.1. Patients

Bone marrow samples from six individuals of paediatric age (1 to 13 years) were used to estimate cell subset proportions. Four patients diagnosed with
400 Idiopathic Thrombocytopenic Purpura (1 from Jerez Hospital and 3 from Niño Jesús Hospital) and two patients with neutropenia (Jerez Hospital). Due to the difficulty in obtaining healthy bone marrow samples from patients of paediatric age, we selected the above as surrogate examples of normal B-cell development. Bone marrow samples were extracted from these patients in order to check
405 for more severe disorders, but they were later diagnosed with B cell-unrelated diseases. Sample inspection further ensured lack of B-line affection. Instances of this can be found in the literature [68, 69].

Appendix A.2. Flow Cytometry

Bone marrow samples were analysed by flow cytometry. This technique
410 measures the expression of the immunophenotypic markers that characterise each maturation stage. Marker expression for both hospitals' data was acquired on a FACSCanto II flow cytometer following the manufacturer's specifications Becton Dickinson (BD) for sample preparation. Samples were stained using an 8-colour panel consisting of the following six fluorochrome-conjugated antibodies
415 provided by BD: CD38 FITC/ CD10 PE/ CD34 PerCP-Cy5-5/ CD19 PE-Cy7/ CD20 APC/ CD45 V-450. This panel allows for the identification of B cell subpopulations [34]. Forward (FSC) and side scatter (SSC) were also measured.

Samples were preprocessed removing debris, doublets and marginal events as is routinely done in clinical and computational flow cytometry [70]. CD19⁺
420 cells were then gated in order to select B lymphocytes [71]. Since the model consists of three B cell populations, we performed k-means clustering on each sample, including all B cell markers, with 3 predefined clusters. The algorithm was initialised randomly and 100 random sets were generated, selecting the one with lower within-cluster variation. Following standard immunophenotyping of

425 B cells [37], clusters were classified into early ($CD45^-/CD10^+$), intermediate
 (430 $CD45^+/CD10^+$) or late ($CD45^+/CD10^-$) B cells. Proportions were then computed
 with respect to the total B lymphocyte count ($CD19^+$ population), which
 correlates with experimental data [38]. Figure A.8 shows the three stages of the
 process. All computations were carried out in RStudio using packages flowCore
 [72] and flowPeaks [73].

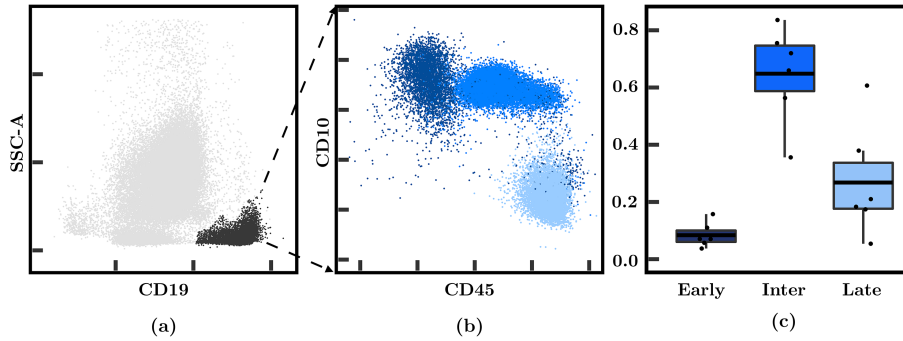


Figure A.8: (a) B Lymphocyte selection in grey ($CD19^+$ population). Y-axis represents cellular complexity, which is low for lymphocytes, and X-axis represents B Lymphocyte surface antigen CD19. (b) Within B population, three clusters were found corresponding to three maturation stages: early, intermediate and late populations. As B cells mature, they gain expression of CD45 antigen and lose expression of CD10 antigen [37]. (c) Boxplots with proportions of each maturation stage from 6 patients displaying mean and 1st and 3rd quartile. Mean values with standard deviations: 0.083 ± 0.009 , 0.648 ± 0.145 , 0.268 ± 0.192 .

Appendix B. Stability analysis for non-trivial equilibria in model A

Appendix B.1. Model A1

We recall the model from Section 3.2.1. From Eq. (22) we obtained the steady states P_i^{A1} for $i = 1, 2, 3$.

Let us consider stability for the equilibrium point P_3^{A2} . We obtain the characteristic equation

$$\lambda^3 + b_2\lambda^2 + b_1\lambda + b_0 = 0, \quad (B.1)$$

where

$$b_2 = \alpha_2 + \alpha_3 - \frac{\alpha_1 \rho_2}{\rho_1}, \quad (\text{B.2a})$$

$$b_1 = \alpha_3 \left(\alpha_2 - \frac{\alpha_1^2 \rho_2}{\rho_1^2} \right), \quad (\text{B.2b})$$

$$b_0 = \frac{\alpha_1 \alpha_3 (\alpha_1 - \rho_1) (\alpha_1 \rho_2 - \alpha_2 \rho_1)}{\rho_1^2}. \quad (\text{B.2c})$$

Using the Routh-Hurwitz Criterion, for P_3^{A1} to be positive and stable we must have

$$b_2 b_1 - b_0 > 0, b_2 > 0, b_0 > 0. \quad (\text{B.3})$$

The positivity conditions found in Eq. (28) yield $b_0 > 0, b_2 > 0$. Furthermore, the stability condition $b_2 b_1 - b_0 > 0$ is satisfied if $\rho_1 \leq \rho_2$. If $\rho_1 > \rho_2$, the stability criterion is equivalent to satisfying either

$$\alpha_1^2 \rho_2 \leq \rho_1 (\alpha_1^2 - \alpha_1 \rho_1 + \alpha_2 \rho_1) \quad (\text{B.4})$$

or

$$\frac{\alpha_2 \rho_1^2 (\alpha_1^2 + \rho_1 (\alpha_2 + \alpha_3)) + \alpha_1^3 \rho_2^2}{\alpha_1 \rho_1} > \alpha_1 \rho_2 (\alpha_T - \rho_1) + \alpha_2 \rho_1 (\rho_1 + \rho_2), \quad (\text{B.5})$$

435 where $\alpha_T = \sum_{i=1}^3 \alpha_i$.

Appendix B.2. Model A2

We recall the model from Section 3.2.2. We obtained in Eq. (29) the steady states P_i^{A2} for $i = 1, 2, 3$.

We use the Routh-Hurwitz Criterion to study the stability of P_3^{A2} . We obtain the characteristic equation

$$\lambda^3 + b_2 \lambda^2 + b_1 \lambda + b_0 = 0, \quad (\text{B.6})$$

where

$$b_2 = \frac{(\alpha_2\alpha_3(\alpha_2 + \alpha_3)\rho_1^2 + \alpha_1\rho_1(\alpha_2^2\rho_1 + \alpha_2\alpha_3(3\rho_1 - 2\rho_2)) + \alpha_3^2(\rho_1 - \rho_2)) - \alpha_1^2(\alpha_3(\rho_1 - \rho_2)\rho_2 + \alpha_2\rho_1(\alpha_3 + \rho_2))}{\rho_1\beta}, \quad (\text{B.7a})$$

$$b_1 = \frac{\alpha_3(\alpha_2^2\alpha_3\rho_1^3 + 2\alpha_1\alpha_2\rho_1^2(\alpha_2\rho_1 + \alpha_3(\rho_1 - \rho_2)) - \alpha_1^3\rho_1(\rho_1 - \rho_2)(\alpha_2 + \rho_2))}{\rho_1^2\beta} + \quad (\text{B.7b})$$

$$+ \frac{\alpha_3\alpha_1^4(\rho_1 - \rho_2)\rho_2}{\rho_1^2\beta} - \frac{\alpha_3\alpha_1^2\rho_1(\alpha_2^2\rho_1 + \alpha_3(\rho_1 - \rho_2)\rho_2 + \alpha_2\rho_1(\alpha_3 - \rho_1 + 2\rho_2))}{\rho_1^2\beta},$$

$$b_0 = \frac{\alpha_1\alpha_3(\alpha_1 - \rho_1)(\alpha_1\rho_2 - \alpha_2\rho_1)}{\rho_1^2}. \quad (\text{B.7c})$$

Positivity conditions for P_3^{A2} as in Eq. (35) and in Eq. (36) yield $b_0 > 0$.

Finally, stability conditions $b_2 > 0$ and $b_2b_1 - b_0 > 0$ result in

$$\frac{(\alpha_2\alpha_3(\alpha_2 + \alpha_3)\rho_1^2 + \alpha_1\rho_1(\alpha_2^2\rho_1 + \alpha_2\alpha_3(3\rho_1 - 2\rho_2)) + \alpha_3^2(\rho_1 - \rho_2)) - \alpha_1^2(\alpha_3(\rho_1 - \rho_2)\rho_2 + \alpha_2\rho_1(\alpha_3 + \rho_2))}{\rho_1\beta} > 0 \quad (\text{B.8a})$$

and

$$\frac{(r_1\rho_1^2 + r_2\rho_1 + r_3(\rho_1 - \rho_2))(r_4\rho_1^3 + r_5\rho_1^2 + r_6(\rho_1 - \rho_2))}{\beta^3} + \alpha_1(\rho_1 - \alpha_1)\rho_1^2(\alpha_1\rho_2 - \alpha_2\rho_1) > 0 \quad (\text{B.8b})$$

where

$$\begin{aligned} r_1 &= \alpha_1\alpha_2^2 + 3\alpha_1\alpha_2\alpha_3 + \alpha_2\alpha_3(\alpha_2 + \alpha_3), \\ r_2 &= -(\alpha_1^2\alpha_2 + 2\alpha_1\alpha_2\alpha_3)\rho_2 - \alpha_1^2\alpha_2\alpha_3, \\ r_3 &= \alpha_1\alpha_3(\alpha_3\rho_1 - \alpha_1\rho_2), \\ r_4 &= \alpha_1^2\alpha_2 + 2\alpha_1\alpha_2^2 + \alpha_2^2\alpha_3, \\ r_5 &= -\alpha_1^2\alpha_2^2 - \alpha_1^2\alpha_2\alpha_3 - 2\alpha_1^2\alpha_2\rho_2, \\ r_6 &= 2\alpha_1\alpha_2\alpha_3\rho_1^2 + \alpha_1^4\rho_2 - \rho_1\alpha_1^2(\alpha_1\alpha_2 + \rho_2(\alpha_1 + \alpha_3)). \end{aligned} \quad (\text{B.8c})$$

Appendix C. Stability analysis for models B

440 Appendix C.1. Model B1

Let us consider Eqs. (8) with last stage signalling $s_\alpha = s_1(t)$ as in Eq. (4), this is, $N = C_3$. The steady states for this model are

$$P_1^{B1} = (0, 0, 0), \quad (\text{C.1a})$$

$$P_2^{B1} = \left(0, \frac{\alpha_3(\alpha_2 - \rho_2)}{k\alpha_2\rho_2}, \frac{\alpha_2 - \rho_2}{k\rho_2} \right), \quad (\text{C.1b})$$

$$P_3^{B1} = \left(\frac{\alpha_3(\alpha_1 - \rho_1)(\alpha_2\rho_1 - \alpha_1\rho_2)}{k\alpha_1\alpha_2\rho_1^2}, \frac{\alpha_3(\alpha_1 - \rho_1)}{k\alpha_2\rho_1}, \frac{\alpha_1 - \rho_1}{k\rho_1} \right). \quad (\text{C.1c})$$

The Jacobian matrix is $J_{B1}(C_1, C_2, C_3) = J_{B1}$ such that

$$J_{B1} = \begin{pmatrix} \rho_1 - \frac{\alpha_1}{C_3k+1} & 0 & \frac{\alpha_1 C_1 k}{(C_3k+1)^2} \\ \frac{\alpha_1}{C_3k+1} & \rho_2 - \frac{\alpha_2}{C_3k+1} & \frac{\alpha_2 C_2 k - \alpha_1 C_1 k}{(C_3k+1)^2} \\ 0 & \frac{\alpha_2}{C_3k+1} & -\frac{\alpha_2 C_2 k + \alpha_3}{(C_3k+1)^2} \end{pmatrix}. \quad (\text{C.2})$$

Substituting P_i^{B1} for $i = 1, 2, 3$ in Eq. (C.2) we obtain the eigenvalues governing linear stability. First, for P_1^{B1} , we obtain the same eigenvalues as for P_1^{A1} , i.e.

$$\lambda_{1,1}^{B1} = -\alpha_3, \quad (\text{C.3a})$$

$$\lambda_{1,2}^{B1} = \rho_1 - \alpha_1, \quad (\text{C.3b})$$

$$\lambda_{1,3}^{B1} = \rho_2 - \alpha_2. \quad (\text{C.3c})$$

For P_2^{B1} we get

$$\lambda_{2,1}^{B1} = \rho_1 - \frac{\alpha_1\rho_2}{\alpha_2}, \quad (\text{C.4a})$$

$$\lambda_{2,2}^{B1} = -\frac{\alpha_3\rho_2 + \sqrt{\alpha_3\rho_2}\sqrt{4\alpha_2 + \alpha_3 - 4\rho_2}}{2\alpha_2}, \quad (\text{C.4b})$$

$$\lambda_{2,3}^{B1} = \frac{\alpha_3\rho_2 - \sqrt{\alpha_3\rho_2}\sqrt{4\alpha_2 + \alpha_3 - 4\rho_2}}{2\alpha_2}. \quad (\text{C.4c})$$

Finally, for P_3^{B1} , we obtain the characteristic equation

$$\lambda^3 + b_2\lambda^2 + b_1\lambda + b_0 = 0, \quad (\text{C.5})$$

where

$$b_2 = \frac{\alpha_2\rho_1 + \alpha_3\rho_1 - \alpha_1\rho_2}{\alpha_1}, \quad (\text{C.6a})$$

$$b_1 = \frac{\alpha_3\rho_1(\alpha_2\rho_1 + \rho_2(\rho_1 - 2\alpha_1))}{\alpha_1^2}, \quad (\text{C.6b})$$

$$b_0 = \frac{\alpha_3(\alpha_1 - \rho_1)\rho_1^2(\alpha_1\rho_2 - \alpha_2\rho_1)}{\alpha_1^3}. \quad (\text{C.6c})$$

Considering positivity conditions for P_2^{B1} and P_3^{B1} , we find that $\lambda_{1,i}^{B1} < 0$ for $i = 1, 2, 3$, and therefore P_1^{B1} is always stable. From the positivity conditions we also get

$$\frac{\rho_1}{\rho_2} > \frac{\alpha_1}{\alpha_2}. \quad (\text{C.7a})$$

which implies $\lambda_{2,1}^{B1} > 0$ and therefore P_2^{B1} is unstable.

Stability of this equilibrium P_3^{B1} can be analysed by the Routh-Hurwitz Criterion from Eq. (B.3). However, given its own positivity conditions, we get $b_0 < 0$, implying P_3^{B1} is always unstable.

Appendix C.2. Model B2

Let us now consider Eqs. (8) with signalling coming from all cellular compartments $s_\alpha = s_1(t)$ as in Eq. (5), this is, $N = \sum_{i=1}^3 C_i$. The steady states of the model are

$$P_1^{B2} = (0, 0, 0), \quad (\text{C.8a})$$

$$P_2^{B2} = \left(0, \frac{\alpha_3(\alpha_2 - \rho_2)}{k(\alpha_2 + \alpha_3)\rho_2}, \frac{\alpha_2(\alpha_2 - \rho_2)}{k(\alpha_2 + \alpha_3)\rho_2} \right), \quad (\text{C.8b})$$

$$P_3^{B2} = \left(\frac{\alpha_3(\alpha_1 - \rho_1)(\alpha_2\rho_1 - \alpha_1\rho_2)}{\rho_1 k \beta}, \frac{\alpha_1\alpha_3(\alpha_1 - \rho_1)}{k\beta}, \frac{\alpha_1\alpha_2(\alpha_1 - \rho_1)}{k\beta} \right), \quad (\text{C.8c})$$

where

$$\beta = (\alpha_2\alpha_3\rho_1 + \alpha_1(\alpha_2\rho_1 + \alpha_3(\rho_1 - \rho_2))). \quad (\text{C.9})$$

The Jacobian matrix of Eqs. (8) with signal s given by Eq. (5) is $J_{B2} = J_{B2}(C_1, C_2, C_3)$ such that

$$J_{B2} = s^2 \begin{pmatrix} C_1 k \alpha_1 - \frac{\alpha_1}{s} + \frac{\rho_1}{s^2} & C_1 k \alpha_1 & C_1 k \alpha_1 \\ \alpha_1 + k R_1 & k R_2 - \frac{\alpha_2}{s} + \frac{\rho_2}{s^2} & k R_2 \\ k R_3 & \alpha_2 + k R_4 & -\alpha_3 - k R_5 \end{pmatrix}, \quad (\text{C.10})$$

where

$$R_1 = C_2(\alpha_1 + \alpha_2) + C_3\alpha_1, \quad (\text{C.11a})$$

$$R_2 = C_2\alpha_2 - C_1\alpha_1, \quad (\text{C.11b})$$

$$R_3 = C_3\alpha_3 - C_2\alpha_2, \quad (\text{C.11c})$$

$$R_4 = C_1\alpha_2 + C_3(\alpha_2 + \alpha_3), \quad (\text{C.11d})$$

$$R_5 = C_1\alpha_3 + C_2(\alpha_2 + \alpha_3). \quad (\text{C.11e})$$

Substituting P_i^{B2} for $i = 1, 2, 3$ in Eq. (C.10) we obtain the eigenvalues governing the linear stability. Specifically, for P_1^{B2} , we again get

$$\lambda_{1,1}^{B2} = -\alpha_3, \quad (\text{C.12a})$$

$$\lambda_{1,2}^{B2} = \rho_1 - \alpha_1, \quad (\text{C.12b})$$

$$\lambda_{1,3}^{B2} = \rho_2 - \alpha_2. \quad (\text{C.12c})$$

For P_2^{B2} , we get the eigenvalues

$$\lambda_{2,1}^{B2} = \rho_1 - \frac{\alpha_1\rho_2}{\alpha_2}, \quad (\text{C.13a})$$

$$\lambda_{2,2}^{B2} = -\frac{\alpha_3^2\rho_2 + \alpha_3\rho_2^2 + h^*(\alpha_2, \alpha_3, \rho_2)}{2\alpha_2(\alpha_2 + \alpha_3)}, \quad (\text{C.13b})$$

$$\lambda_{2,3}^{B2} = \frac{-\alpha_3^2\rho_2 - \alpha_3\rho_2^2 + h^*(\alpha_2, \alpha_3, \rho_2)}{2\alpha_2(\alpha_2 + \alpha_3)}. \quad (\text{C.13c})$$

where $h^* = h^*(\alpha_2, \alpha_3, \rho_2)$ such that

$$h^* = \sqrt{\alpha_3\rho_2} \sqrt{4\alpha_2(\alpha_2^2 + \alpha_2(2\alpha_3 - \rho_2) + \alpha_3(\alpha_3 - 2\rho_2)) + \alpha_3(\alpha_3 - \rho_2)^2}. \quad (\text{C.14})$$

Finally, for P_3^{B2} , we obtain the characteristic equation

$$\lambda^3 + b_2\lambda^2 + b_1\lambda + b_0 = 0, \quad (\text{C.15})$$

where

$$b_2 = \frac{\alpha_2 \alpha_3 \rho_1^2 (\alpha_2 + \alpha_3 + \rho_1) + \alpha_1 \rho_1 (\alpha_2^2 \rho_1 + \alpha_2 \alpha_3 (\rho_1 - 2\rho_2))}{\alpha_1 \beta} + \quad (\text{C.16a})$$

$$+ \frac{\alpha_3^2 (\rho_1 - \rho_2) - \alpha_1^2 (\alpha_2 \rho_1 + \alpha_3 (\rho_1 - \rho_2)) \rho_2}{\alpha_1 \beta},$$

$$b_1 = \frac{\alpha_3 \rho_1 (\alpha_2 \rho_1^2 (\alpha_3 \rho_1 + \alpha_2 (\alpha_3 + \rho_1)) + \alpha_1^3 (\rho_1 - \rho_2) \rho_2)}{\alpha_1^2 \beta} + \quad (\text{C.16b})$$

$$- \frac{\alpha_1 \alpha_2 \rho_1 (\rho_1^2 - 2\alpha_3 \rho_2 - \rho_1 \rho_2) - \alpha_1^2 (\alpha_2 \rho_1^2 + (\alpha_3 + \rho_1) (\rho_1 - \rho_2) \rho_2)}{\alpha_1^2 \beta},$$

$$b_0 = \frac{\alpha_3 (\alpha_1 - \rho_1) \rho_1^2 (\alpha_1 \rho_2 - \alpha_2 \rho_1)}{\alpha_1^3}. \quad (\text{C.16c})$$

Every equilibrium stability is influenced by the positivity conditions of the other points. From the positivity of P_2^{B2} , we get that

$$\alpha_2 > \rho_2. \quad (\text{C.17})$$

Two different scenarios arise from the positivity conditions of P_3^{B2} ; either

$$\beta > 0, \quad (\text{C.18a})$$

$$\alpha_1 > \rho_1, \quad (\text{C.18b})$$

$$\alpha_2 \rho_1 > \alpha_1 \rho_2; \quad (\text{C.18c})$$

or

$$\beta < 0, \quad (\text{C.19a})$$

$$\alpha_1 < \rho_1, \quad (\text{C.19b})$$

$$\alpha_2 \rho_1 < \alpha_1 \rho_2. \quad (\text{C.19c})$$

Whenever Eq. (C.18) holds, equilibrium P_1^{B2} is stable (mainly $\alpha_1 < \rho_1$, as Eq.(C.17) is true whenever $P_2^{B2} > 0$). Moreover, equilibrium P_2^{B2} would also be stable whenever Eq. (C.19) holds and also

$$|\mathcal{R}(h^*)| < \alpha_3^2 \rho_2 + \alpha_3 \rho_2^2 \quad (\text{C.20})$$

where h^* is defined as in Eq. (C.14). However, the stability of P_1^{B2} and P_2^{B2} is biologically uninteresting. Focusing on the non-trivial state, with the above
450 constraints Eq.(C.18) or Eq.(C.19) and the Routh-Hurtwitz criterion, we have $b_0 < 0$. Therefore, P_3^{B2} is positive but always unstable.

Appendix D. Summary of stability conditions

We summarise in Table D.3 the conclusions of the mathematical analysis regarding stability of the non-trivial state.

Steady State	Model A1 $s_\rho = s_1, s_\alpha = 1$	Model A2 $s_\rho = s_2, s_\alpha = 1$	Model B1 $s_\rho = 1, s_\alpha = s_1$	Model B2 $s_\rho = 1, s_\alpha = s_2$
P_1^j	Unstable	Unstable	Stable	Conditionally stable
P_2^j	Unstable	Conditionally stable	Unstable	Conditionally stable
P_3^j	Conditionally Stable	Conditionally Stable	Unstable	Unstable

Table D.3: Steady-state stability for every model from Eq. (6) under conditions of positivity of the non-trivial steady state. Index j stands for the four models considering the different feedback regulations: *A1* for cell proliferation regulation, all cell feedback; *A2* for proliferation regulation, late cell feedback; *B1* for transition rate regulation, late cell feedback; and *B2* for transition rate regulation, all cell feedback.

455 References

References

- [1] S. Doulatov, F. Notta, E. Laurenti, J. E. Dick, Hematopoiesis: a human perspective, *Cell stem cell* 10 (2) (2012) 120–136. doi:10.1016/j.stem.2012.01.006.
- 460 [2] E. Laurenti, B. Göttgens, From haematopoietic stem cells to complex differentiation landscapes, *Nature* 553 (7689) (2018) 418–426. doi:10.1038/nature25022.
- [3] B. Alberts, D. Bray, J. Lewis, M. Raff, K. Roberts, J. Watson, *Molecular Biology of the Cell*, 4th Edition, Garland, 2002. doi:10.1016/0307-4412(94)90059-0.
- 465

- [4] T. W. LeBien, T. F. Tedder, B lymphocytes: how they develop and function, *Blood* 112 (5) (2008) 1570–1580. doi:10.1182/blood-2008-02-078071.
- [5] E. Steliarova-Foucher, M. Colombet, L. A. Ries, F. Moreno, A. Dolya, 470 F. Bray, P. Hesselning, H. Y. Shin, C. A. Stiller, S. Bouzbid, et al., International incidence of childhood cancer, 2001–10: a population-based registry study, *The Lancet Oncology* 18 (6) (2017) 719–731. doi:10.1002/cncr.20910.
- [6] T. Reya, S. J. Morrison, M. F. Clarke, I. L. Weissman, Stem cells, cancer, 475 and cancer stem cells, *Nature* 414 (6859) (2001) 105–111. doi:10.1038/35102167.
- [7] G. Clapp, D. Levy, A review of mathematical models for leukemia and lymphoma, *Drug Discovery Today: Disease Models* 16 (2015) 1–6. doi:10.1016/j.ddmod.2014.10.002.
- [8] Pujol-Menjouet, L., Blood cell dynamics: Half of a century of modelling, 480 *Math. Model. Nat. Phenom.* 11 (1) (2016) 92–115. doi:10.1051/mmnp/2016111106.
- [9] T. Lorenzi, A. Marciniak-Czochra, T. Stiehl, A structured population model of clonal selection in acute leukemias with multiple maturation stages, *Journal of Mathematical Biology* 79 (5) (2019) 1587–1621. doi: 485 10.1007/s00285-019-01404-w.
- [10] A. Marciniak-Czochra, T. Stiehl, W. Wagner, Modeling of replicative senescence in hematopoietic development, *Aging* 1 (8) (2009) 723–732. doi:10.18632/aging.100072.
- [11] I. Roeder, Quantitative stem cell biology: computational studies in the 490 hematopoietic system, *Current Opinion in Hematology* 13 (4) (2006) 222–228. doi:10.1097/01.moh.0000231418.08031.48.

- [12] S. Viswanathan, P. W. Zandstra, Towards predictive models of stem cell fate, *Cytotechnology* 41 (2/3) (2003) 75–92. doi:10.1023/a:1024866504538.
- 495
- [13] V. V. Ganusov, J. Auerbach, Mathematical modeling reveals kinetics of lymphocyte recirculation in the whole organism, *PLoS Computational Biology* 10 (5) (2014) e1003586. doi:10.1371/journal.pcbi.1003586.
- [14] T. Stiehl, A. Marciniak-Czochra, Characterization of stem cells using mathematical models of multistage cell lineages, *Mathematical and Computer Modelling* 53 (7-8) (2011) 1505–1517. doi:10.1016/j.mcm.2010.03.057.
- 500
- [15] M. C. Mackey, R. Rudnicki, Global stability in a delayed partial differential equation describing cellular replication, *Journal of Mathematical Biology* 33 (1) (1994) 89–109. doi:10.1007/bf00160175.
- [16] D. Dingli, F. Michor, Successful therapy must eradicate cancer stem cells, *Stem Cells* 24 (12) (2006) 2603–2610. doi:10.1634/stemcells.2006-0136.
- 505
- URL <https://doi.org/10.1634/stemcells.2006-0136>
- [17] G. Shahaf, S. Zisman-Rozen, D. Benhamou, D. Melamed, R. Mehr, B cell development in the bone marrow is regulated by homeostatic feedback exerted by mature b cells, *Frontiers in immunology* 7 (2016) 77. doi:10.3389/fimmu.2016.00077.
- 510
- [18] S. Hu, O. A. Smirnova, F. A. Cucinotta, A biomathematical model of lymphopoiesis following severe radiation accidents-potential use for dose assessment, *Health physics* 102 (4) (2012) 425–436. doi:10.1097/HP.0b013e318240593d.
- 515
- [19] N. L. Komarova, Principles of regulation of self-renewing cell lineages, *PloS one* 8 (9). doi:10.1371/journal.pone.0072847.
- [20] E. Manesso, J. Teles, D. Bryder, C. Peterson, Dynamical modelling of haematopoiesis: an integrated view over the system in homeostasis and
- 520

under perturbation, *Journal of the Royal Society Interface* 10 (80) (2013) 20120817. doi:10.1098/rsif.2012.0817.

- 525 [21] D. S. Jones, M. Plank, B. D. Sleeman, *Differential equations and mathematical biology*, Chapman and Hall/CRC, 2009. doi:10.1201/9781420083583.
- [22] K. Murphy, C. Weaver, *Janeway's immunobiology*, Garland science, 2016. doi:10.1201/9781315533247.
- [23] T. W. LeBien, Fates of human b-cell precursors, *Blood, The Journal of the American Society of Hematology* 96 (1) (2000) 9–23. doi:10.1182/blood.V96.1.9.
- 530 [24] D. H. Fuerstinger, F. Kappel, S. Thijssen, N. W. Levin, P. Kotanko, A model of erythropoiesis in adults with sufficient iron availability, *Journal of mathematical biology* 66 (6) (2013) 1209–1240. doi:10.1007/s00285-012-0530-0.
- 535 [25] T. Walenda, T. Stiehl, H. Braun, J. Fröbel, A. D. Ho, T. Schroeder, T. W. Goecke, B. Rath, U. Germing, A. Marciniak-Czochra, et al., Feedback signals in myelodysplastic syndromes: increased self-renewal of the malignant clone suppresses normal hematopoiesis, *PLoS computational biology* 10 (4). doi:10.1371/journal.pcbi.1003599.
- 540 [26] T. Stiehl, N. Baran, A. D. Ho, A. Marciniak-Czochra, Clonal selection and therapy resistance in acute leukaemias: mathematical modelling explains different proliferation patterns at diagnosis and relapse, *Journal of The Royal Society Interface* 11 (94) (2014) 20140079–20140079. doi:10.1098/rsif.2014.0079.
- 545 [27] W. Wang, T. Stiehl, S. Raffel, V. T. Hoang, I. Hoffmann, L. Poisa-Beiro, B. R. Saeed, R. Blume, L. Manta, V. Eckstein, et al., Reduced hematopoietic stem cell frequency predicts outcome in acute myeloid leukemia,

Haematologica 102 (9) (2017) 1567–1577. doi:10.3324/haematol.2016.163584.

- 550 [28] F. Knauer, T. Stiehl, A. Marciniak-Czochra, Oscillations in a white blood cell production model with multiple differentiation stages, Journal of Mathematical Biology 80 (3) (2020) 575–600. doi:10.1007/s00285-019-01432-6.
- [29] H. Jumaa, R. W. Hendriks, M. Reth, B cell signaling and tumorigenesis, Annu. Rev. Immunol. 23 (2005) 415–445. doi:10.1146/annurev.immunol.23.021704.115606.
- [30] R. Mehr, G. Shahaf, A. Sah, M. Cancro, Asynchronous differentiation models explain bone marrow labeling kinetics and predict reflux between the pre-and immature b cell pools, International immunology 15 (3) (2003) 301–312. doi:10.1093/intimm/dxg025.
- 560 [31] O. A. Smirnova, S. Hu, F. A. Cucinotta, Analysis of the lymphocytopoiesis dynamics in nonirradiated and irradiated humans: a modeling approach, Radiation Research 181 (3) (2014) 240–250. doi:10.1667/RR13256.1.
- [32] R. Mostolizadeh, Z. Afsharnezhad, A. Marciniak-Czochra, Mathematical model of chimeric anti-gene receptor (car) t cell therapy with presence of cytokine, Numerical Algebra, Control & Optimization 8 (1) (2018) 63. doi:10.3934/naco.2018004.
- 565 [33] O. León-Triana, S. Sabir, G. F. Calvo, J. Belmonte-Beitia, S. Chulián, Á. Martínez-Rubio, M. Rosa, A. Pérez-Martínez, M. R. Orellana, V. M. Pérez-García, Car t cell therapy in b-cell acute lymphoblastic leukaemia: Insights from mathematical models, arXiv preprint.arXiv:2003.10236.
- 570 [34] J. Van Dongen, L. Lhermitte, S. Böttcher, J. Almeida, V. Van der Velden, J. Flores-Montero, A. Rawstron, V. Asnafi, Q. Lecomte, P. Lucio, et al., Euroflow antibody panels for standardized n-dimensional flow cytomet-

- 575 ric immunophenotyping of normal, reactive and malignant leukocytes,
Leukemia 26 (9) (2012) 1908–1975. doi:10.1038/leu.2012.120.
- [35] A. Marciniak-Czochra, T. Stiehl, A. D. Ho, W. Jger, W. Wagner, Modeling
of asymmetric cell division in hematopoietic stem cells—regulation of self-
renewal is essential for efficient repopulation, Stem Cells and Development
580 18 (3) (2009) 377–386. doi:10.1089/scd.2008.0143.
- [36] T. Stiehl, A. Marciniak-Czochra, Stem cell self-renewal in regeneration and
cancer: insights from mathematical modeling, Current Opinion in Systems
Biology 5 (2017) 112–120. doi:10.1016/j.coisb.2017.09.006.
- [37] E. van Lochem, V. van der Velden, H. Wind, J. te Marvelde, N. West-
585 erdaal, J. van Dongen, Immunophenotypic differentiation patterns of nor-
mal hematopoiesis in human bone marrow: Reference patterns for age-
related changes and disease-induced shifts, Cytometry 60B (1) (2004) 1–13.
doi:10.1002/cyto.b.20008.
- [38] P. Lúcio, A. Parreira, M. van den Beemd, E. van Lochem, E. van Wering,
590 E. Baars, A. Porwit-MacDonald, E. Bjorklund, G. Gaipa, A. Biondi, A. Or-
fao, G. Janossy, J. van Dongen, J. S. Miguel, Flow cytometric analysis of
normal b cell differentiation: a frame of reference for the detection of min-
imal residual disease in precursor-b-all, Leukemia 13 (3) (1999) 419–427.
doi:10.1038/sj.leu.2401279.
- 595 [39] D. Dingli, J. M. Pacheco, Modeling the architecture and dynamics of
hematopoiesis, Wiley Interdisciplinary Reviews: Systems Biology and
Medicine 2 (2) (2009) 235–244. doi:10.1002/wsbm.56.
- [40] H. Kraus, S. Kaiser, K. Aumann, P. Bönelt, U. Salzer, D. Vestweber,
600 M. Erlacher, M. Kunze, M. Burger, K. Pieper, H. Sic, A. Rolink, H. Eibel,
M. Rizzi, A feeder-free differentiation system identifies autonomously pro-
liferating b cell precursors in human bone marrow, The Journal of Im-
munology 192 (3) (2014) 1044–1054. doi:10.4049/jimmunol.1301815.

- [41] R. Maddaly, G. Pai, S. Balaji, P. Sivaramakrishnan, L. Srinivasan, S. S. Sunder, S. F. Paul, Receptors and signaling mechanisms for b-lymphocyte activation, proliferation and differentiation—insights from both in vivo and in vitro approaches, *FEBS letters* 584 (24) (2010) 4883–4894. doi:10.1016/j.febslet.2010.08.022.
- [42] J. J. O’Shea, M. Gadina, R. M. Siegel, Cytokines and cytokine receptors, in: *Clinical immunology*, Elsevier, 2019, pp. 127–155. doi:10.1016/B978-0-7020-6896-6.00009-0.
- [43] G. Petkau, M. Turner, Signalling circuits that direct early b-cell development, *Biochemical Journal* 476 (5) (2019) 769–778. doi:10.1042/BCJ20180565.
- [44] A. Marciniak-Czochra, A. Mikelić, T. Stiehl, Renormalization group second-order approximation for singularly perturbed nonlinear ordinary differential equations, *Mathematical Methods in the Applied Sciences* 41 (14) (2018) 5691–5710. doi:10.1002/mma.5107.
- [45] T. Guillaume, D. B. Rubinstein, M. Symann, Immune reconstitution and immunotherapy after autologous hematopoietic stem cell transplantation, *Blood, The Journal of the American Society of Hematology* 92 (5) (1998) 1471–1490. doi:10.1182/blood.V92.5.1471.
- [46] D. Leitenberg, J. M. Rapoport, B. R. Smith, B-cell precursor bone marrow reconstitution after bone marrow transplantation, *American journal of clinical pathology* 102 (2) (1994) 231–236. doi:10.1093/ajcp/102.2.231.
- [47] J. E. Talmadge, E. Reed, K. Ino, A. Kessinger, C. Kuszynski, D. Heimann, M. Varney, J. Jackson, J. M. Vose, P. J. Bierman, Rapid immunologic reconstitution following transplantation with mobilized peripheral blood stem cells as compared to bone marrow, *Bone marrow transplantation* 19 (2) (1997) 161–172. doi:10.1038/sj.bmt.1700626.

- 630 [48] A. Parrado, S. Casares, J. Prieto, M. Carmona, A. Vaquero, J. Rodriguez-Fernandez, Repopulation of circulating t, b and nk lymphocytes following bone marrow and blood stem cell transplantation, *Hematology and cell therapy* 39 (6) (1997) 301–306. doi:10.1007/s00282-997-0301-3.
- [49] G. J. Deenen, I. Van Balen, D. Opstelten, In rat b lymphocyte genesis sixty
635 percent is lost from the bone marrow at the transition of nondividing pre-b cell to sigm+ b lymphocyte, the stage of ig light chain gene expression, *European journal of immunology* 20 (3) (1990) 557–564. doi:10.1002/eji.1830200315.
- [50] Y.-H. Park, D. G. Osmond, Dynamics of early b lymphocyte precursor
640 cells in mouse bone marrow: proliferation of cells containing terminal deoxynucleotidyl transferase, *European journal of immunology* 19 (11) (1989) 2139–2144. doi:10.1002/eji.1830191125.
- [51] H. E. Skipper, S. Perry, Kinetics of normal and leukemic leukocyte populations and relevance to chemotherapy, *Cancer Research* 30 (6) (1970)
645 1883–1897.
- [52] A. K. Abbas, A. H. Lichtman, S. Pillai, *Cellular and molecular immunology*, Elsevier Health Sciences, 1994.
- [53] S. C. Bendall, K. L. Davis, E.-a. D. Amir, M. D. Tadmor, E. F. Simonds, T. J. Chen, D. K. Shenfeld, G. P. Nolan, D. Peer, Single-cell trajectory
650 detection uncovers progression and regulatory coordination in human b cell development, *Cell* 157 (3) (2014) 714–725. doi:10.1016/j.cell.2014.04.005.
- [54] J. G. Monroe, G. Bannish, E. M. Fuentes-Panana, L. B. King, P. C. Sandel, J. Chung, R. Sater, Positive and negative selection during b
655 lymphocyte development, *Immunologic research* 27 (2-3) (2003) 427–442. doi:10.1385/IR:27:2-3:427.

- [55] D. G. Osmond, Population dynamics of bone marrow b lymphocytes, *Immunological reviews* 93 (1) (1986) 103–124. doi:10.1111/j.1600-065x.1986.tb01504.x.
- 660 [56] P. Clark, D. Normansell, D. Innes, C. Hess, Lymphocyte subsets in normal bone marrow, *Blood* 67 (6) (1986) 1600–1606. doi:10.1182/blood.V67.6.1600.1600.
- [57] C. Andreoni, D. Rigal, M. Bonnard, J. Bernaud, Phenotypic analysis of a large number of normal human bone marrow sample by flow cytometry, *Blut* 61 (5) (1990) 271–277. doi:10.1007/BF01732876.
- 665 [58] C. W. Caldwell, E. Poje, M. A. Helikson, B-cell precursors in normal pediatric bone marrow, *American journal of clinical pathology* 95 (6) (1991) 816–823. doi:10.1093/ajcp/95.6.816.
- [59] E. M. Rego, A. B. Garcia, S. R. Viana, R. P. Falcão, Age-related changes of lymphocyte subsets in normal bone marrow biopsies, *Cytometry: The Journal of the International Society for Analytical Cytology* 34 (1) (1998) 22–29. doi:10.1002/(SICI)1097-0320(19980215)34:1<22::AID-CYT04>3.0.CO;2-G.
- 670 [60] C. Nombela-Arrieta, M. G. Manz, Quantification and three-dimensional microanatomical organization of the bone marrow, *Blood Advances* 1 (6) (2017) 407–416. doi:10.1182/bloodadvances.2016003194.
- [61] Kleiveland, Charlotte R., *Peripheral Blood Mononuclear Cells*, Springer International Publishing, Cham, 2015, pp. 161–167. doi:10.1007/978-3-319-16104-4_15.
- 680 [62] G. Caocci, M. Greco, G. La Nasa, Bone marrow homing and engraftment defects of human hematopoietic stem and progenitor cells, *Mediterranean journal of hematology and infectious diseases* 9 (1). doi:10.4084/MJHID.2017.032.

- [63] H. Kawamoto, H. Wada, Y. Katsura, A revised scheme for developmental
685 pathways of hematopoietic cells: the myeloid-based model, *International
immunology* 22 (2) (2010) 65–70. doi:10.1093/intimm/dxp125.
- [64] A. Wilson, E. Laurenti, G. Oser, R. C. van der Wath, W. Blanco-Bose,
M. Jaworski, S. Offner, C. F. Dunant, L. Eshkind, E. Bockamp, et al.,
690 Hematopoietic stem cells reversibly switch from dormancy to self-renewal
during homeostasis and repair, *Cell* 135 (6) (2008) 1118–1129. doi:10.
1016/j.cell.2008.10.048.
- [65] L. Biasco, D. Pellin, S. Scala, F. Dionisio, L. Basso-Ricci, L. Leonardelli,
S. Scaramuzza, C. Baricordi, F. Ferrua, M. P. Cicalese, et al., In vivo
tracking of human hematopoiesis reveals patterns of clonal dynamics during
695 early and steady-state reconstitution phases, *Cell stem cell* 19 (1) (2016)
107–119. doi:10.1016/j.stem.2016.04.016.
- [66] K. Busch, K. Klapproth, M. Barile, M. Flossdorf, T. Holland-Letz, S. M.
Schlenner, M. Reth, T. Höfer, H.-R. Rodewald, Fundamental properties
of unperturbed haematopoiesis from stem cells in vivo, *Nature* 518 (7540)
700 (2015) 542–546. doi:10.1038/nature14242.
- [67] R. R. Hardy, P. W. Kincade, K. Dorshkind, The protean nature of cells in
the b lymphocyte lineage, *Immunity* 26 (6) (2007) 703–714. doi:10.1016/
j.immuni.2007.05.013.
- [68] Z. Ahmad, N. Durrani, T. Hazir, Bone marrow examination in itp in chil-
705 dren: is it mandatory?, *Journal of the College of Physicians and Surgeons-
Pakistan: JCPSP* 17 (6) (2007) 347–349. doi:06.2007/jcpsp.347349.
- [69] H. Zafar, S. Anwar, M. Faizan, S. Riaz, Clinical features and outcome in
paediatric newly diagnosed immune thrombocytopenic purpura in a ter-
tiary care centre, *Pakistan journal of medical sciences* 34 (5) (2018) 1195.
710 doi:doi:10.12669/pjms.345.15687.

- [70] Y. Saeys, S. Van Gassen, B. N. Lambrecht, Computational flow cytometry: helping to make sense of high-dimensional immunology data, *Nature Reviews Immunology* 16 (7) (2016) 449. doi:10.1038/nri.2016.56.
- 715 [71] G. Finak, M. Langweiler, M. Jaimes, M. Malek, J. Taghiyar, Y. Korin, K. Raddassi, L. Devine, G. Obermoser, M. L. Pekalski, et al., Standardizing flow cytometry immunophenotyping analysis from the human immunophenotyping consortium, *Scientific reports* 6 (1) (2016) 1–11. doi:10.1038/srep20686.
- 720 [72] F. Hahne, N. LeMeur, R. R. Brinkman, B. Ellis, P. Haaland, D. Sarkar, J. Spidlen, E. Strain, R. Gentleman, flowcore: a bioconductor package for high throughput flow cytometry, *BMC bioinformatics* 10 (1) (2009) 106. doi:10.1186/1471-2105-10-106.
- 725 [73] Y. Ge, S. C. Sealfon, flowpeaks: a fast unsupervised clustering for flow cytometry data via k-means and density peak finding, *Bioinformatics* 28 (15) (2012) 2052–2058. doi:10.1093/bioinformatics/bts300.